URANUS

Jay T. Bergstralh
Ellis D. Miner
Mildred Shapley Matthews

Editors

With 84 collaborating authors

THE UNIVERSITY OF ARIZONA PRESS
TUCSON

About the cover:

The front cover is a Voyager montage of Uranus encircled by its "classical" narrow rings, as seen from above its innermost satellite, Miranda (foreground). It is intended to represent the tangible elements of the Uranian system: the planet itself, the ring system and the regular satellite system. The appearance of the planet is dominated by a nearly featureless global cloud cover, probably consisting of condensed methane; its blue-green tint is caused by strong absorption of red photons by gaseous methane in the extensive atmosphere above the clouds. The narrow rings in this montage barely suggest the rich variety of dynamic phenomena and physical properties detected in the ring system through groundbased observations and by various experiments on Voyager. While Miranda is not truly typical of Uranus' major satellites, its rugged surface, evidence of an astonishing degree of tectonic activity on such a small body, is suggestive of the range of geological and evolutionary processes on these satellites. Not seen are ten minor satellites, two of them embedded in the ring system, discovered by Voyager.

The back cover is a schematic of the Uranian magnetosphere (Krimigis et al. 1986), illustrating its principal features: bow shock, magnetopause, boundary layer, dayside cusp, plasma sheet, radiation belts, satellite sweeping and the extended atomic hydrogen corona surrounding the planet, as derived from Voyager experiments. This is intended to represent what might be called the intengible elements of the Uranian system. Although these are its largest structures, their properties (and even their existence) were speculative before the Voyager encounter. Some peculiarities arise from interactions of the solar wind with the strongly offset and tilted, rotating planetary magnetic field. Not illustrated are interactions (e.g., aurorae) between the magnetosphere and the planet's atmosphere.

The University of Arizona Press

This book is printed on acid-free, archival-quality paper.
Manufactured in the United States of America.

96 95 94 93 92 91 6 5 4 3 2 1

Library of Congress Cataloging-in-Publication Data

Uranus / Jay T. Bergstralh, Ellis D. Miner, Mildred Shapley Matthews, editors : with 84 collaborating authors.
p. cm. — (Space science series)
Includes bibliographical references and index.
ISBN 0-8165-1208-6 (ci : acid free paper)
1. Uranus (Planet) I. Bergstralh, Jay T. II. Miner, Ellis D., 1937– . III. Matthews, Mildred Shapley. IV. Series.
QB681.U378 1990
523.4'7—dc20 90-21185
CIP

British Library Cataloguing in Publication data are available.

WAVE-PARTICLE INTERACTIONS IN THE MAGNETOSPHERE OF URANUS

W. S. KURTH, D. A. GURNETT
The University of Iowa

F. L. SCARF
TRW Space and Technology Group

and

F. V. CORONITI
University of California, Los Angeles

The Voyager 2 encounter of Uranus provided observations of plasma waves in and near the magnetosphere. These data, the first from Uranus, are the only direct information on wave-particle interactions at this planet for many years to come. The observations include electrostatic waves upstream of the bow shock, turbulence in the shock, Bernstein emissions and whistler-mode waves in the magnetosphere, broadband electrostatic noise in the magnetotail, and many other types of plasma waves which have yet to be clearly identified. Each of these types of waves exist in a plasma environment which both supports the growth of the waves and is modified by interactions with the waves. Wave-particle interactions provide the channels through which the waves can accelerate, scatter or thermalize the plasmas. The most spectacular example in the case of Uranus is the extremely intense whistler-mode activity in the inner magnetosphere which is the source of strong pitch-angle diffusion. The resulting electron precipitation is sufficient to produce the auroral emissions observed by Voyager. The strong diffusion, however, presents the problem of supplying electrons in the range 5 to 40 keV to support losses to the atmosphere.

I. INTRODUCTION

The magnetosphere of Uranus is the site of intense plasma-wave activity (Gurnett et al. 1986) and exhibits evidence of strong wave-particle interactions important in the generation of the aurora observed by the Voyager ultraviolet sensor (UVS) and in the energy budget of the magnetosphere. The magnetosphere is also the site of a number of weaker plasma waves that interact with the local plasma, but that are of lesser importance in the overall dynamics of the system. In this chapter, the observations of plasma waves and instabilities observed by the Voyager plasma wave receiver in and near the Uranian magnetosphere are reviewed. An attempt is made to assess the impact of the observed plasma waves on the plasma- and energetic-particle populations resident in the various regions of the magnetosphere. Finally, the role of the waves in the various magnetospheric processes is discussed.

The Uranian magnetosphere comprises the Uranian magnetic field (chapter by Ness et al., Ness et al. 1986), a thermal plasma, and various energetic-particle populations composed almost exclusively of protons (chapters by Belcher et al. and Cheng et al.; Bridge et al. 1986; Krimigis et al. 1986*a*; Stone et al. 1986). The outer boundary of the magnetosphere, the magnetopause, was crossed by Voyager 2 at a distance of about 18 R_U on the day side of Uranus; the bow shock was detected at a distance of about 23.7 R_U. The highly asymmetric pressure of the supersonically flowing solar wind is responsible for the formation of a long magnetic tail, analogous to other magnetospheres. The trajectory of Voyager 2 was specifically designed for a subsequent Neptune encounter; it left the dawn flank of the Uranus tail at a distance of about 80.5 R_U. One of the most spectacular discoveries of the Voyager flyby of Uranus was the $\sim 60°$ tilt of the magnetic dipole with respect to the rotational axis and an offset of nearly a third of the planetary radius (Ness et al. 1986). This unexpected field configuration dismantled earlier speculations on the form of the Uranian magnetosphere (cf. Siscoe 1975; Hill 1984). The unusual dipole configuration leads to many asymmetries in the magnetosphere, one of the most obvious being the highly asymmetric radio emission pattern (chapter by Desch et al.; Warwick et al. 1986; Kaiser et al. 1987). The resulting implication is that the plasma populations responsible for driving the radio emissions find suitable conditions for existence on the nightside, southern magnetic hemisphere.

Figure 1 provides an overview of the Uranus encounter as viewed by the plasma wave spectrum analyzer from before the inbound bow shock to the first encounters of the bow shock on the outbound leg of the trajectory (Gurnett et al. 1986). Upstream wave activity and the bow-shock signature can be seen early on January 24; these waves are discussed in Sec. II. Little wave activity is seen after the shock crossing until shortly after noon on January 24 when Bernstein emissions are observed in the 1.0− and 1.78-kHz channels

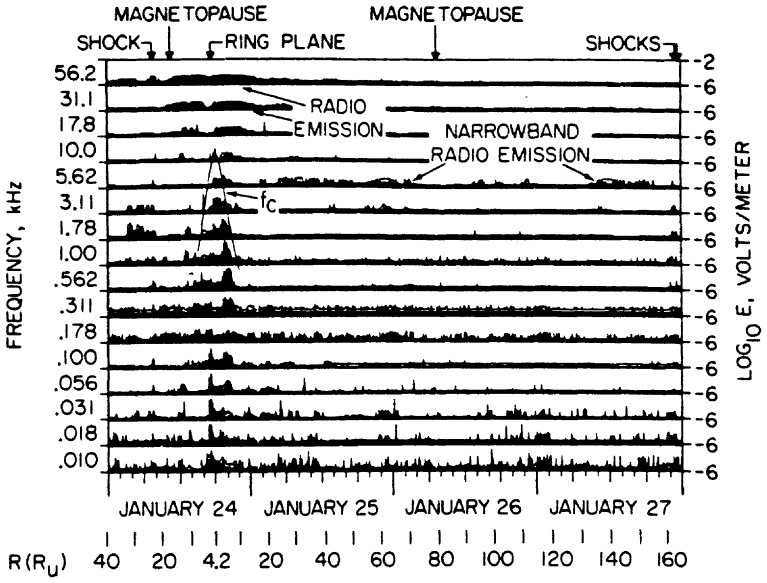

Fig. 1. An overview of the plasma wave observations at Uranus from just prior to the inbound bow-shock crossing to the first of the outbound shocks (figure from Gurnett et al., *Science*, Vol. 233,106, 4 July 1986; Copyright 1986 by the AAAS). The bulk of the wave activity is in the inner magnetosphere.

at about 1300 SCET (spacecraft event time, referring to the time in UTC of an event at the spacecraft). Other Bernstein wave activity can be found closer to Uranus, above the electron cyclotron frequency f_c contour which is based on the intensity (B) of the magnetic field provided by the offset tilted dipole (OTD) magnetic field model (Ness et al. 1986) by f_c (Hz) = $28|B|$ (nT). (The Bernstein emissions will be discussed in Sec. III.) As in the case of the other planetary magnetospheres (Kurth 1985), the bulk of the plasma wave activity is found in the inner magnetosphere, from about 1500 through 2100 SCET on the same day, and is located below the f_c contour. A comparison with the plasma and energetic particle observations (chapters by Belcher et al. and Cheng et al.) shows that this is the same time interval when plasma and energetic particle fluxes were high. This band of wave activity, which is the most intense whistler-mode activity observed thus far in the magnetospheres of the outer planets (Gurnett et al. 1986; Scarf et al. 1987), is discussed fully in Sec. IV, specifically with regard to the potential for strong pitch-angle scattering provided by these waves. Some weak activity below about 100 Hz can be found during the magnetotail traversal after about 2200 SCET on January 24. These waves, tentatively identified as broadband electrostatic noise, are discussed in Sec. V.

Throughout this chapter, reference is made to the Voyager 2 plasma wave receiver. While it is inappropriate to describe it in great detail here, it is important to understand that this instrument is composed of two sections. Most of the results presented herein come from the 16-channel spectrum analyzer, which returns every 4 s an amplitude in each of 16 fixed-frequency channels logarithmically spaced in frequency from 10 Hz to 56.2 kHz. The other instrument section (a wideband waveform receiver) returns a continuous 10- or 48-s digitized sample of the waveform in the frequency range from about 40 Hz to 12 kHz. The wideband receiver requires a data rate of 115.2 kilobits per second. Because these data must compete for limited tape-recorder resources, only short snapshots at infrequent intervals can be afforded. However, these snapshots provide extremely high temporal and spectral resolution and greatly assist in the identification of various wave emissions.

The Voyager plasma wave receiver has only the shared use of the planetary radio astronomy antennas for sensors, which it uses as a balanced dipole with an effective length of 7.07 m. Hence, any identification of an emission as electrostatic or electromagnetic can be made only by (1) the frequency of the emission with respect to critical frequencies of the plasma; (2) the spectral and temporal variations of the emission (electrostatic waves tend to be burstier than electromagnetic waves); and (3) analogy with similar emissions observed in the terrestrial magnetosphere where electric and magnetic observations have confirmed the mode of propagation for many of the various emissions. For a complete discussion of the instrumentation, see Scarf and Gurnett (1977).

It should be pointed out that the planetary radio astronomy receiver also measured waves in the vicinity of Uranus (Warwick et al. 1986) and has contributed greatly to our understanding of magnetospheric processes. The bulk of the radio astronomy observations are at higher frequencies and, hence, are of freely propagating radio waves. The chapter by Desch et al. reviews the radio emissions in detail. This chapter avoids the consideration of most aspects of the radio emissions to avoid duplication.

II. UPSTREAM WAVES AND BOW-SHOCK TURBULENCE

Besides radio emissions, which can often be observed great distances from a planetary magnetosphere, upstream plasma waves are among the first indicators to an approaching spacecraft of the existence of the interaction of the solar wind with the magnetosphere. In the outer heliosphere, the solar-wind plasma is tenuous and the solar magnetic field is very weak, on the order of 0.1 nT (Ness et al. 1986), and the sonic and Alfvénic Mach numbers are very large (Bagenal et al. 1987). At these solar distances the magnetic field is largely azimuthal. Voyager 2, approaching the nose of the Uranian magnetosphere, was expected to observe a high-Mach-number, thin, quasi-

perpendicular shock. In this configuration of trajectory and magnetic-field orientation, it is likely that the spacecraft will not be magnetically connected to the magnetosphere or its bow shock for a very long distance upstream. Nevertheless, Voyager 2 did observe extensive upstream wave activity in addition to the bow shock itself (Gurnett et al. 1986). Energetic particles were also observed in the upstream region by the Low Energy Charged Particle (LECP) investigation on Voyager 2 (chapter by Cheng et al.; Krimigis et al. 1986*a*; Mauk et al. 1987; Krimigis et al. 1988). As discussed below, it is likely that the energetic particles are associated with the observed upstream waves.

Observations of Upstream Langmuir Waves

The plasma wave instrument observed an extensive region upstream of the bow shock with Langmuir waves of up to 100 $\mu V\ m^{-1}$. These waves were seen over an interval of more than a day (Figure 2), when Voyager 2 was up to 80 R_U from Uranus, and appeared predominantly in the 1.78- and 3.11-kHz channels. Based on solar-wind plasma observations (Bridge et al. 1986; Bagenal et al. 1987) 2 to 3 kHz would be very close to the electron plasma frequency f_p, where $f_p[\text{Hz}] = 8980\sqrt{n_e}$. Here, n_e is the local electron density in cm^{-3}. The bursty nature of the waves is quite apparent in Fig. 2, even though the plotted values represent 144-s averages. Structure is seen in these emissions at the 4-s resolution of the spectrum analyzer.

The upstream wave activity depicted in Fig. 2 indicates that Voyager 2 was magnetically connected to the Uranian bow shock for significant periods of time prior to crossing the bow shock, since the waves near f_p are driven by electrons which have been accelerated at the bow shock and flow into the upstream solar wind. Given the nominal magnetic-field configuration, which is almost purely azimuthal at Uranus, Voyager could only detect the waves if extraordinary field direction changes occurred, that is, if the solar magnetic field possessed a large radial component, or if the spacecraft were very close to the Uranian bow shock. In fact, it is likely both conditions occurred. For the extended interval of upstream activity on January 23, there is evidence of a substantial radial component of the field (Krimigis et al. 1988), providing the condition of magnetic connection to the bow shock, even if the shock was a considerable distance away.

On the other hand, the upstream activity observed prior to the bow shock encounter on January 24 was primarily due to the close proximity of the spacecraft to the shock, making the field orientation less important. It is remarkable that the upstream waves on January 24 occurred over an extended interval of about 4 hr. During the 4-hr interval, Voyager was generally connected with the bow shock (Krimigis et al. 1988); the close proximity of the boundary during this time considerably relaxes the geometrical constraints on the magnetic field. During both intervals of upstream wave activity, Krimigis et al. (1988) reported enhancements of protons with $28 < E < 137$ keV

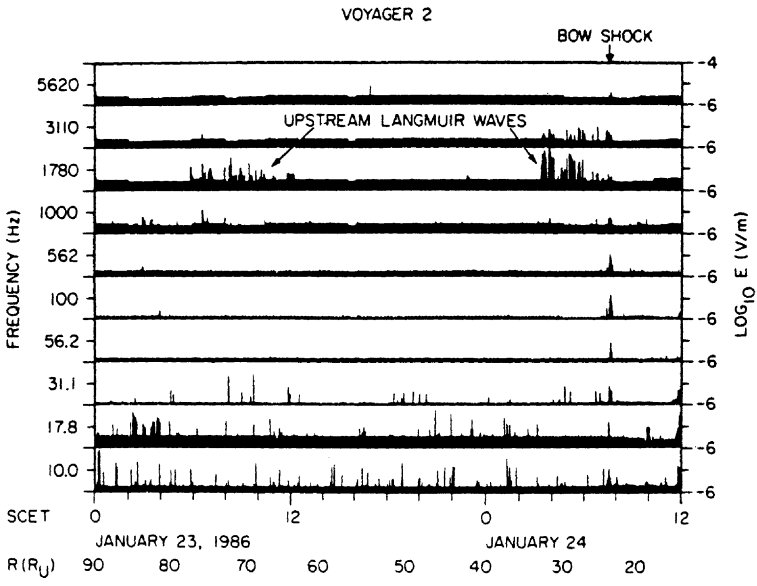

Fig. 2. The upstream portion of the Voyager 2 plasma wave data set showing extensive Langmuir wave activity at distances as far out as 80 R_U.

coming from the direction of Uranus, but no evidence of electrons. Although electrons are expected to be responsible for the Langmuir waves, it is possible that these electrons have energies between the 28 keV lower limit of the LECP and the 6 keV upper limit of PLS (Plasma Science Instrument) as was the case at Jupiter (Gurnett et al. 1981). Another possible source for the Langmuir waves is the ion beams themselves. Given a solar-wind temperature of about 3 eV (Bagenal et al. 1987), the 28-keV ions observed would appear as a very cold beam; such a distribution could excite ion Buneman modes, in particular the electron plasma oscillation branch.

Waves near f_p in the region upstream of planetary bow shocks are quite common and have been studied extensively at the Earth and Jupiter (Scarf et al. 1971; Gurnett and Frank 1975; Filbert and Kellogg 1979; Gurnett et al. 1981). These waves are often called electron plasma oscillations or Langmuir waves. They are often quite narrowbanded and are typically quite intense, among the most intense waves observed in the vicinity of a planetary magnetosphere.

No detailed spectra of the Uranian Langmuir waves were obtained because of the limited number of wideband frames. Terrestrial and Jovian studies show that the waves are quite narrowbanded and bursty. Terrestrial observations with spacecraft having wave magnetic-field sensors also show that these emissions are electrostatic in nature; there is no detectable magnetic

component to the waves. By analogy, the same is assumed to be true of the Uranian examples. The fact that the emissions sometimes appear in two adjacent channels in Fig. 2 does not necessarily mean the Uranian emissions have a broad spectrum; more likely the emissions lie somewhere between the center frequencies of the adjacent channels and the filter skirt response to the off-center frequencies is sufficient to account for the intensities in both channels.

Gurnett et al. (1981) discussed the detailed spectral and temporal behavior of the Jovian Langmuir waves. There, very short bursts of waves occurred at frequencies just above and below the primary line at f_p. Gurnett et al., suggested that the bursts were of an intensity that was close to exceeding the criterion for the creation of solitons, wherein the electric field increases and plasma is forced outward due to the ponderomotive force. This process proceeds very rapidly until the solitons collapse. Nicholson et al. (1978) provide a thorough review of soliton theory. However, it is likely that heat flows are strong enough to explain the waves at frequencies well separated from f_p without resorting to the nonlinear theory.

The dispersion relation for Langmuir waves assuming weak turbulence is

$$f^2 = f_p^2(1 + 3k^2\lambda_D^2) \tag{1}$$

where k is the wave number and λ_D is the Debye length. The growth of the Langmuir waves is one of the classical problems in plasma physics in that it involves a very simple double-humped velocity distribution function. Nevertheless, there is still no satisfactory explanation of the generation mechanism. The basic idea is clear, however. The bow shock serves as a place where electrons can be accelerated and directed back upstream into the solar wind. This beam of electrons forms a double hump in the electron distribution function when added to the ambient solar-wind electron distribution. It is easily shown that such a distribution is a source of free energy and is unstable to Langmuir waves. The theory still does not explain the nonlinear beam stabilization processes that keep the Langmuir waves from completely disrupting the beam (Papadopoulos et al. 1974). It is also possible for waves near f_p to be driven by a strong electron heat flux in the solar wind as observed at Jupiter (Moses et al. 1984), or by the observed high-energy ion beams as suggested above.

Other waves common in the upstream region at Earth and Jupiter include ion-acoustic waves, which, after being Doppler shifted by the solar-wind flow, can occur at frequencies up to $f_{max} = v_{sw}/2\pi\lambda_D$ where v_{sw} is the solar-wind velocity. There is little or no evidence for these emissions in the Uranus data set, however. The 48-s waveform samples obtained once or twice per day provide the best opportunity to observe such sporadic emissions, but there is no evidence for ion-acoustic waves in those samples. Besides the low-

duty cycle for the waveform data, relatively intense low-frequency interference covering a broad frequency range centered on about 200 Hz would make it very difficult to discern such emissions were they present. Numerous low-frequency bursts, some of which can be seen in Fig. 2, appear in the spectrum analyzer data set. It is quite likely that some of these bursts correspond to ion-acoustic waves. However, the spacecraft-attitude control system interferes with the plasma wave instrument at frequencies below about 1 kHz, so it is impossible to ascertain whether any of the randomly occurring bursts are due to real plasma wave signals. Ion-acoustic waves are not restricted to the vicinity of planetary bow shocks or interplanetary shocks; Kurth et al. (1979*c*) showed evidence of these emissions in the solar wind well separated from any bow shock or interplanetary shocks.

Bow-Shock Turbulence

Voyager crossed the bow shock once on the inbound leg of the Uranus trajectory; that shock crossing has been studied in detail by Bagenal et al. (1987). Shortly after 0730 SCET the plasma wave instrument detected broadband electric-field enhancements which resemble the type of spectrum observed at the other planetary bow shocks (Gurnett et al. 1986); however, the wave signature was unusually irregular and diffuse (Scarf et al. 1987). The spectrum was consistent with the lower characteristic frequencies of the solar-wind plasma due to the very low plasma density (0.05 cm^{-3}) and weak magnetic field (0.19 nT) in the solar wind in the vicinity of Uranus at the time of the Voyager encounter (Bagenal et al. 1987).

On the outbound leg, numerous bow-shock crossings were recorded by the Voyager magnetometer and plasma instruments (Ness et al. 1986; Bridge et al. 1986). While some of the shock crossings listed by these two initial reports agree rather well, the two lists contain substantial differences. The plasma wave investigation also observed signatures associated with some of the reported crossings (Gurnett et al. 1986); other crossings had no clear signature in the wave data. It is not presently clear whether some of the bow shocks simply do not show a wave signature (this would be an exceptional result) or whether the initial lists contain questionable identifications. All bow-shock crossings reported by both the magnetometer and plasma investigations show a clear plasma wave signature. One possible explanation for the shocks which show little or no wave signature is that the turbulence is so sporadic and impulsive that the 4-s spectrum analyzer sweep is too slow to catch the increases (Scarf et al. 1981).

As reported by Bagenal et al. (1987), the conditions for the inbound bow-shock crossing were ideal for a quasi-perpendicular shock, where the normal to the shock surface was nearly perpendicular to the impinging solar-wind magnetic field. In contrast, the outbound crossings occurred on the dawn-side flank of the magnetotail and the nominal field orientation leads to a quasi-parallel shock configuration. Striking differences are seen between

the spectra of plasma wave turbulence in the inbound versus outbound shock crossings (see, e.g., Fig. 2 of Scarf et al. 1987). Figure 3 shows 1-min average and peak spectra for the inbound shock as well as a shock observed near 2300 SCET on January 27 1986 on the outbound leg. The high-frequency portions of the two spectra are similar, with waves extending up to a few kHz, consistent with the solar-wind plasma frequency. At frequencies between about 30 and 100 Hz, however, the outbound bow shock shows almost no wave activity at all. There is evidence in the outbound shock of shock-associated emissions in the 10-Hz channel. The other outbound shocks exhibiting some wave signature tend to follow the trend of the shock displayed in the right-hand panel of Fig. 3. Whether the difference in the inbound and outbound spectra is due to the quasi-perpendicular/quasi-parallel differences, or to some other factor, is not known at this time.

The modes responsible for the spectra in Fig. 3 have not been identified with any degree of certainty at this time. Only the electric-field spectrum provides any clues, because Voyager has neither wave magnetic-field sensor nor polarization measurements for plasma waves, and there are no wideband

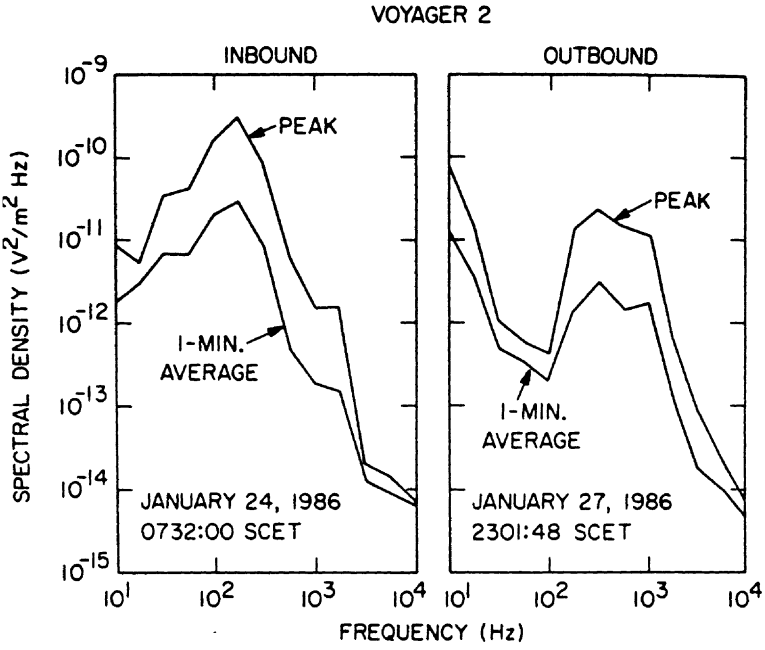

Fig. 3. A comparison of the plasma wave spectra obtained during the inbound bow-shock crossing (left panel) and one of the outbound bow-shock crossings (right panel). The primary difference is the notch in the spectrum in the range of 30 to 100 Hz observed near the outbound shock.

data available within the shock. Data from other planets may provide some clues, assuming conditions at Uranus are not drastically different from those at Jupiter or Saturn. One possibility for the frequency component centered near 0.5 kHz in Fig. 3 is a Buneman mode (Moses et al. 1988). These intermediate-frequency waves in the inbound spectrum could also be ion-acoustic-like modes (Scarf et al. 1979; Scarf et al. 1981). As pointed out by Melrose (1980), the Buneman instability transforms to the ion-acoustic instability in a manner very similar to the way the two-stream instability makes the transition to the bump-on-tail. The bandwidth of the wave spectrum broadens as one moves from a cold to warm plasma regime. The lower-frequency component near 10 Hz in the outbound spectrum in Fig. 3 is likely to be a whistler mode. A magnetic-field strength of about 0.5 nT (Ness et al. 1986) gives an electron cyclotron frequency of about 14 Hz.

The wave turbulence in shocks has been related to particle acceleration, at least in the Earth's bow shock (see Tsurutani and Rodriguez 1981, and references therein; Lee 1982). It has also been speculated that the wave turbulence in a collisionless shock is responsible for heating the plasma. More recent studies (Goodrich and Scudder 1984; Scudder et al. 1986*b*,*c*; Mellott 1986) suggest that the plasma waves in the terrestrial bow shock are not required to produce the observed amount of heating; the potential drop across the shock is sufficient, at least in the reported cases (Scudder et al. 1986*b*). Moses et al. (1985,1988) found, however, that waves in the shock foot at Jupiter and Saturn are responsible for the observed electron heating through electrostatic waves generated by reflected ions. Detailed analyses of the Uranian shocks have been initiated only recently. Preliminary calculations indicate that the wave amplitudes are too weak (at least at the inbound shock) to explain the heating. This is because the high ion temperatures of ~4 eV (Bagenal et al. 1987) restrict the ion-beam instability (Moses et al. 1989).

III. BERNSTEIN EMISSIONS

Bernstein emissions, also commonly referred to as $(n + 1/2)f_c$ emissions, are very common in planetary magnetospheres, including those of Earth, Jupiter and Saturn (Kennel et al. 1970; Kurth et al. 1980*a*; Kurth et al. 1983). The preferred location for these emissions in the terrestrial magnetosphere is beyond the plasmapause at the magnetic equator (Christiansen et al. 1978). At Jupiter the bands are very tightly confined to magnetic latitudes of one or two degrees and are observed almost exclusively inside of about 23 R_J. Saturn's Bernstein waves are also located in the inner magnetosphere, but show a weaker magnetic latitude confinement than at Jupiter.

The Bernstein emissions are electrostatic waves that are driven by a variety of free energy sources having a positive slope with respect to the velocity perpendicular to the magnetic field in the electron distribution function. They can have intensities up to several mV m^{-1} at the Earth. For many years,

Bernstein waves were thought to be the primary source of pitch-angle scattering of terrestrial plasma-sheet electrons forming the diffuse aurora (Lyons 1974). Belmont et al. (1983) have cast some doubt on this conclusion; their analysis was based on an extensive survey of $(n + 1/2)f_c$ band intensities in the terrestrial magnetosphere.

It was not surprising to find the familiar Bernstein waves in the Uranian magnetosphere (Gurnett et al. 1986). Kurth et al. (1987) reported the emissions as a prominent part of the plasma wave spectrum at Uranus, second only to the whistler-mode hiss and chorus observed in the inner Uranian magnetosphere. (The whistler-mode emissions are discussed in Sec.IV.) This section presents a review of some of the characteristics of the Bernstein emissions observed at Uranus and elsewhere.

Observations of Bernstein Waves at Uranus

Figure 4 summarizes the locations, frequencies and intensities of the Bernstein waves observed in the Uranian magnetosphere (Kurth et al. 1987). One of the first indications of the extreme tilt of the magnetic dipole at Uranus was the occurrence of the most prominent example of Bernstein emissions at a distance of about 11.5 R_U in the dayside magnetosphere. In Fig. 4, this event can be seen near 1315 SCET on January 24. It is visible primarily in the 1- and 1.78-kHz channels. Other examples closer to Uranus are visible in Fig. 4. If the magnetic dipole had been aligned with the rotation axis, the strongest emissions would have occurred near the ring-plane crossing (1716 SCET). The 1315 SCET event very nearly corresponds to the magnetic-equator crossing for the offset tilted dipole, and the Voyager spacecraft did not cross the magnetic equator again at smaller Uranus ranges.

Details of the 1315 SCET event are shown in Fig. 5. In this expanded view of the plasma wave spectrum from 311 Hz through 3.11 kHz, it is clear that the Bernstein waves cover a fairly broad range in frequencies and are bursty, showing order-of-magnitude intensity variations on times scales of a few seconds. The burstiness of these emissions is evidence that the waves are electrostatic, but a true determination of the electrostatic character of the waves is not possible with the Voyager sensor. The amplitudes of these emissions are about 100 $\mu V\ m^{-1}$.

A few words are in order about the spectral character of the Bernstein emissions. Numerous observations in the terrestrial magnetosphere (Kennell et al. 1970; Scarf et al. 1973) make it clear that the emissions are composed of one or more narrow bands lying between harmonics of the electron cyclotron frequency. The $(n + 1/2)f_c$ nomenclature stems from the spacing between the bands of about f_c and the fact that the bands are between the actual harmonics of f_c, even though they very often do not lie exactly half-way in between.

Hubbard and Birmingham (1978) classified several types of occurrences of the $(n + 1/2)f_c$ bands. Generally speaking, the bands appear in families.

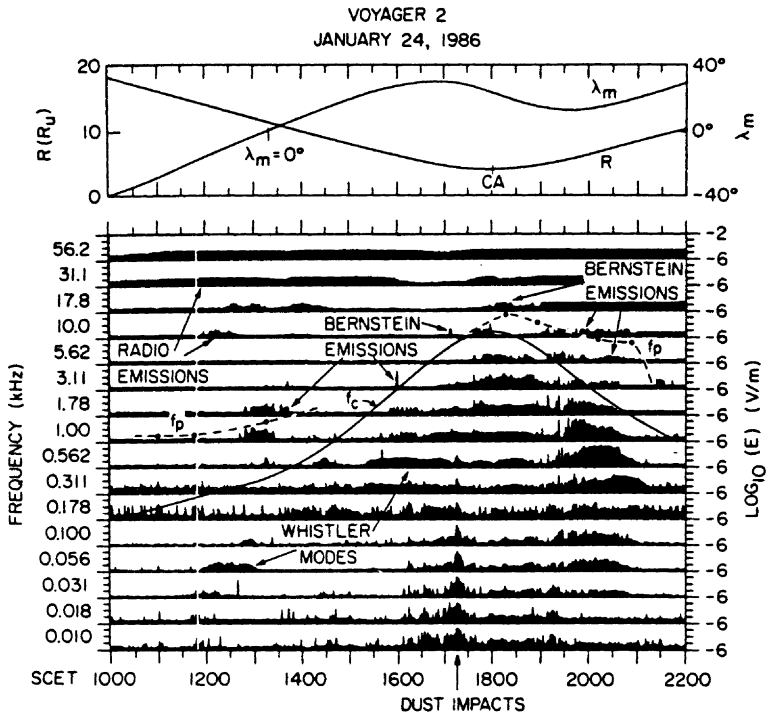

Fig. 4. A summary of the electrostatic Bernstein wave emissions observed by Voyager 2 at Uranus (Kurth et al. 1987). The bursty emissions above the f_c contour and below the smoothly varying radio emissions are the electrostatic waves. Notice that the inner magnetospheric pass occurred at rather high magnetic latitudes (top panel), where the growth of the Bernstein waves is not expected to be large.

Often, the bands start just above f_c and appear between each harmonic between f_c and f_p, with the lowest bands having the highest intensity. Sometimes, the harmonic band including the upper hybrid resonance frequency $f_{uhr} = \sqrt{f_p^2 + f_c^2}$ contains a band and this one can often be the most intense (Kurth et al. 1979*b*). When the upper hybrid band is observed, the lower harmonics may not be observable at all. There are also cases where only the lowest $(3f_c/2)$ harmonic is observed.

From Fig. 5 it is clear that the Voyager spectrum analyzer did not resolve the different harmonic components. The higher-resolution wideband measurements would have been quite useful here, if they had been available. From the spread in frequency, it is apparent that emissions are present in several of the bands. Because of the finite filter bandwidths of the spectrum analyzer, the actual number of harmonics present is indeterminable. Kurth et

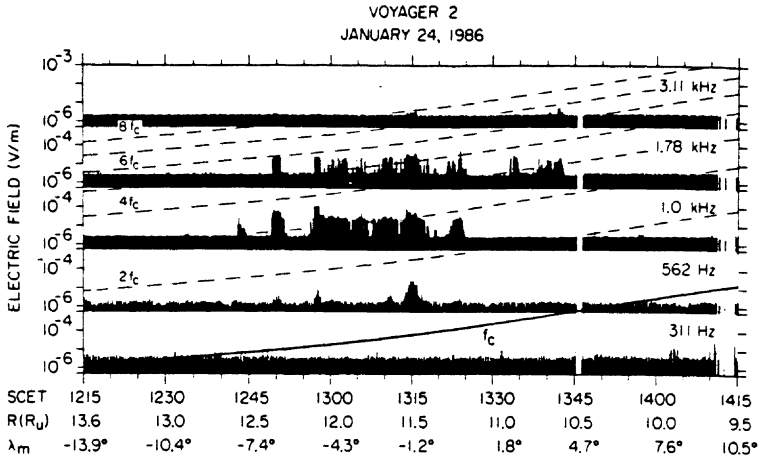

Fig. 5. An expanded view of the Bernstein emissions observed near the magnetic equator at 11.5 R_U (Kurth et al. 1987). Notice the bursty nature of the waves and the broad frequency extent. This spectrum is likely composed of narrowband emissions between the first three or four harmonics of the electron cyclotron frequency.

al. (1987) suggest that the strongest band, which would include f_{uhr}, is between 3 and $4f_c$, which would place the upper hybrid band near $7f_c/2$.

Bursty emissions in the channels at or above the electron cyclotron frequency profile (solid line in Fig. 4) provide additional evidence for Bernstein emissions at Uranus. Generally, the remaining emissions are rather weak, averaging about 30 $\mu V\ m^{-1}$. They occur primarily near closest approach and on the outbound leg, and are weak compared to the event in Fig. 5, most likely owing to the less favorable conditions for growth above or below the magnetic equator. The conditions for growth to reasonable amplitudes require large temporal growth rates and sufficiently long path lengths through the region of growth. Various studies (cf. Engle and Kennel 1984) have shown that Bernstein waves tend to be trapped at low magnetic latitudes and propagate primarily in azimuth about the planet. Conditions near the magnetic equator best support the growth of waves to large amplitudes. Had Voyager traversed the magnetic equator closer to Uranus than in the Fig. 5 event, it is likely even more intense waves would have been observed.

Theory of the Bernstein Emissions

An in-depth discussion of the theory behind the Bernstein emissions is given by Ashour-Abdalla and Kennel (1978*a*, and references therein). Here, only a few aspects of the generation of the waves are discussed. The dispersion relation governing the emissions is given by Harris (1959). A necessary condition for growth of the waves is a region in the electron velocity distri-

bution $f(v)$ for which $\partial f/\partial v_\perp$ is positive. The first such distribution function proposed was a severe and unrealistic ring distribution with a delta function (Fredricks 1971). Young et al. (1973) showed that the addition of cold electrons greatly reduced the requirements on the electron distribution function which would support wave growth. Soon, the canonical distribution used to model the $(n + 1/2)f_c$ emissions was one in which there was a loss-cone feature in the hot electrons with a core of cold electrons. Ashour-Abdalla and Kennel (1978*a*,*b*) and Hubbard and Birmingham (1978) showed that by varying the ratio of hot to cold electrons and their temperatures one could generate waves similar to those observed.

Shortly thereafter Rönnmark et al. (1978) and Kurth et al. (1979*a*) showed qualitative agreement between observed $(n + 1/2)f_c$ spectra and theoretical growth-rate calculations. Kurth et al. (1980*b*) further showed that the actual form of the distribution is not critical; not only can loss-cone features provide the free energy for the emissions, but other distributions with a positive $\partial f/\partial v_\perp$ feature (such as a hot shell) might also serve.

Perhaps it is this relative insensitivity to the actual form of the distribution function which enables the ubiquitous occurrence of these electrostatic waves in planetary magnetospheres with dramatically different plasma and energy sources.

Barbosa and Kurth (1980) derived an expression for the critical flux of anisotropic electrons ($E_\perp > E_\parallel$) required to amplify the $3f_c/2$ band by 10 *e*-foldings. Kurth et al. (1987) modified the expression for Uranus to the following form:

$$Tj_\perp^* = 5.4 \times 10^4 \left(\frac{T/T_c}{4}\right)^2 \left(\frac{T_c}{30\ \text{eV}}\right) \text{cm}^{-2}\text{s}^{-1}\text{sr}^{-1} \qquad (2)$$

where T is the electron temperature and T_c is the temperature of the cold, background electrons. They used 0.23 G as the surface field of Uranus, $R_U = 25{,}600$ km, $n_c = 3.9 \times 10^{-2}$ cm^{-3}, $R = 11.5$, $\delta\tilde{\omega} = 0.1$, and $\tilde{\omega} = 1.5$ in the formulation by Barbosa and Kurth (1980). Kurth et al. (1987) used a value of 10 to 30 eV for the background electron temperature, typical of temperatures measured by PLS closer to the planet (Bridge et al. 1986; McNutt et al. 1987). When evaluated at the magnetic equator crossing by Voyager 2 (see Fig. 5), the above expression yields a critical flux of 3×10^5 cm^{-2}s^{-1}, assuming an effective solid angle of about 2π. The flux measured by Bridge et al. (1986) was nearly the same value.

This good agreement with theory is somewhat compromised by the subsequent report of Sittler et al. (1987). They found that because the electrons measured by PLS in the vicinity of the magnetic-equator crossing are very close to threshold, there is no solid evidence for <1 keV electrons at this location unless they are as cold as 1 eV. The electron density derived from

the existence of the Bernstein emissions by Kurth et al. (1987) is almost an order of magnitude greater than that reported by Sittler et al. (1987) for the same time period. The tentative conclusion is that there are significant fluxes of electrons either near 1 eV or higher than the 6-keV limit of the PLS. The resonant electron energy of a few hundred eV reported by Kurth et al. (1987) may hold in the inner magnetosphere, but the lack of observed plasma fluxes at 11.5 R_U (Sittler et al. 1987) makes it difficult to confirm the resonant energy for the Fig. 5 event.

Lyons (1974) recognized that strong electron cyclotron emissions can pitch-angle scatter electrons of a few keV and, therefore, represent a viable means of precipitating electrons into the diffuse aurora. While Belmont et al. (1983) discounted Lyons' conclusion that these electrostatic waves alone could account for the diffuse aurora at Earth, the ability of the waves to pitch-angle scatter electrons remains. Hence, the Bernstein waves at Uranus must be viewed as a scattering mechanism. The low amplitudes reported are possibly misleading since it is likely that more intense emissions lie near the magnetic equator in the inner magnetosphere not sampled by Voyager. Unfortunately, the importance of the scattering due to these waves cannot be assessed on the basis of the incomplete survey provided by the Voyager 2 trajectory.

Recently, Kurth et al. (1990) reported observations of nonthermal continuum radiation trapped in the magnetosphere of Uranus. These radio emissions are at such low frequencies ($\leq$3 kHz) that they are confined within the magnetospheric cavity. Kurth et al. identified the upper hybrid band associated with the Bernstein emissions at 1315 SCET (Fig. 5) as the source for the continuum radiation. This identification can be made because (1) the continuum was observed just prior to the magnetic-equator crossing where the upper hybrid waves were observed; (2) the frequency of the continuum and upper hybrid waves are similar; and (3) the upper hybrid waves are known to be the source of continuum radiation at the Earth.

Density Profile Based on Bernstein Emissions

Since the frequency range over which the $(n + 1/2)f_c$ emissions can be observed is generally between f_c and f_{uhr}, an analysis of the occurrence of these electrostatic emissions can provide some independent information on the electron density. Kurth et al. (1987) made use of this technique to derive a partial plasma density profile for the Uranian magnetosphere; their results are shown by the dashed line in Fig. 4. The derivation is based on knowing that the upper frequency limit for the Bernstein bands is approximately the upper hybrid resonance frequency. Since the cyclotron frequency is well known, this yields the plasma frequency from which the plasma density can be determined. For example, at the magnetic-equator crossing the highest frequency and most intense band is likely to be the upper hybrid band. Kurth

et al. deduced a plasma frequency of 1.6 kHz, or a plasma density of about 0.03 cm^{-3} for the center of this event at 1315 SCET on January 24. It is possible that only the lower harmonic $(n + 1/2)f_c$ bands are being observed, in which case 0.03 cm^{-3} is only a lower limit to the density at this time.

In the region after closest approach the transition from the bursty emissions above f_c to the smooth radio emissions at higher frequencies provides another set of information on the density. Here, it was necessary to assume a propagation mode for the radio emissions to know if the cutoff of the radio waves was the left-hand ordinary (L-O) or right-hand extraordinary (R-X) cutoff (or whether the cutoff frequency was the plasma frequency or f_R, the right-hand cutoff) (Stix 1962) where

$$f_R = \frac{f_c}{2} + \left(f_p^2 + \frac{f_c^2}{4}\right)^{1/2}. \tag{3}$$

Kurth et al. assumed the radio waves are propagating in the R-X mode to derive the profile shown in Fig. 4. This choice provided consistency with the PLS observations of the density during the post-closest approach interval and has been confirmed by recent radio astronomy studies (Kaiser et al. 1988).

The dashed-line profile in Fig. 4 is based primarily on the dots located at various points on the profile. At those times, some specific piece of information provided constraints on the density. The dashed line between these dots is a smooth curve and as such may not be accurate.

IV. WHISTLER-MODE EMISSIONS

The dominant plasma wave phenomenon in the Uranian magnetosphere is the whistler-mode emissions below f_c in the inner Uranian magnetosphere (Gurnett et al. 1986). In this section, the emissions are described, the implications for pitch-angle scattering implied by the observed intensities are discussed, and the inferred precipitating fluxes are compared with independent measurements of the diffusion coefficient.

Observations of Whistler-Mode Waves

Figure 6 summarizes the plasma wave spectrum for the inner magnetosphere of Uranus. The spectrum analyzer data shown here covers the radial distance range inward of about 8 R_U. It is dominated by the intense band of emissions which occur consistently below the f_c contour. As in previous figures, the f_c contour is based on the OTD model field strength given by Ness et al. (1986). The other signals present below the cyclotron frequency include the sharply peaked emission at the ring-plane crossing (1716 SCET) due to the effect of micron-sized dust particles impacting on the spacecraft (Gurnett

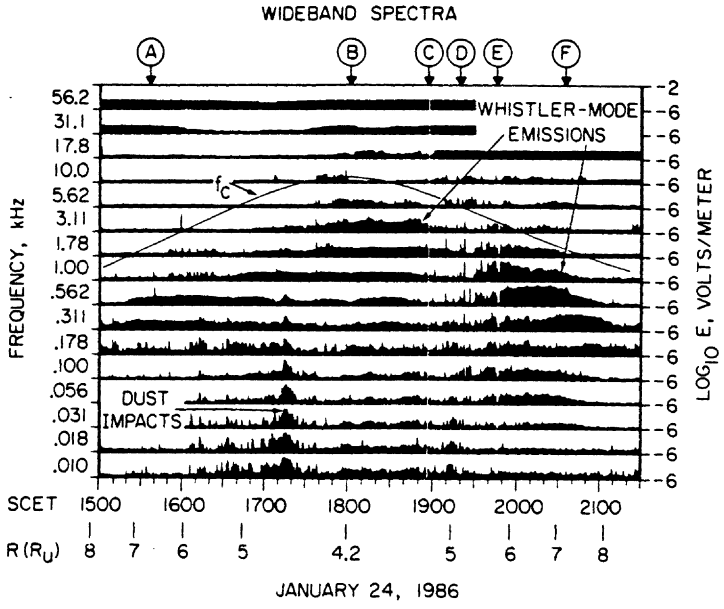

Fig. 6. An overview of the extensive occurrence of whistler-mode waves, seen here below the f_c contour (figure from Gurnett et al., *Science*, Vol. 233,106, 4 July 1986; Copyright 1986 by the AAAS).

et al. 1987). A band of signals at 56 and 100 Hz between about 1930 and 2030 SCET has been tentatively identified as lower hybrid resonance emissions by Coroniti et al. (1987).

The whistler-mode emissions in Fig. 6 extend from as high as 20 to 50% of the electron cyclotron frequency down to as low as $0.1\,f_c$. The emissions are observable over almost the entire interval plotted except for several minutes around 1930 SCET. At that time numerous bursty emissions are observed but the whistler-mode emissions are clearly missing. An obvious inbound-outbound asymmetry is also apparent; the outbound interval between 1950 and 2100 SCET contains the most intense whistler-mode emissions. Scarf et al. (1987) label these as the most intense whistler-mode emissions observed in any outer planet magnetosphere.

At the top of Fig. 6, six times are labeled by the letters *A* through *F*. These refer to times when brief high spectral and temporal resolution snapshots of the frequency-time spectrum were obtained with the Voyager wideband receiver. The panels in Fig. 7 show the detailed frequency-time variations of the whistler-mode emissions at these six times. (Plate 3 in the color section is the color version of Fig. 7.) The most striking characteristic is the

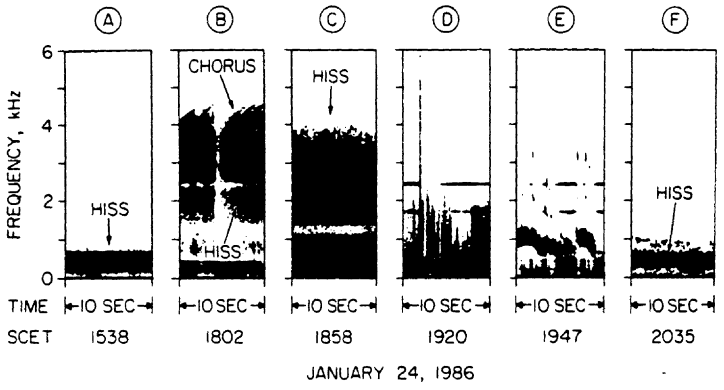

Fig. 7. A series of 10-s snapshots of the detailed frequency-time character of the whistler-mode emissions represented in Fig. 6 (figure adapted from Fig. 5 of Gurnett et al. 1986). Panel *B* shows an example of chorus growing out of the top of the hiss band and Panel *D* shows the very bursty and, as yet, unexplained emissions near 1930 SCET where the whistler band is interrupted (see Fig. 6). A color version of this figure (Plate 3) can be found in the color section of this book.

variation in bandwidth as f_c rises and falls. (Note that the spectrograms in Fig. 7 and Plate 3 have linear frequency scales instead of the logarithmic frequency scale used in Fig. 6.)

Panels *A*, *C*, *E* and *F* all show the presence of an almost featureless band of "hiss." Audio recordings reveal a considerable amount of structure not readily apparent in the spectrograms, particularly for frames *E* and *F*. Grabbe (1988*a*,*b*) has attempted to explain some of this structure as a propagation effect of whistler waves on the resonance cone passing through density and/or magnetic-field inhomogeneities. Panel *B* shows the presence of discrete rising tones growing out of the hiss band at lower frequencies. These tones are easily recognized as typical "chorus" elements, strikingly similar to those observed at Earth (Helliwell 1965) and Jupiter (Coroniti et al. 1984). Panel *D* is taken from the above-mentioned whistler band gap and consists of very bursty, probably electrostatic emissions (Kurth et al. 1986). An identification of these modes would lead to some very interesting clues about the source of the whistler band gap, but is beyond the scope of this review.

Figure 8 shows a detailed amplitude versus frequency slice through Panel *F* in Plate 3 (Fig. 7), averaged over 0.6 s. It is clear from this illustration that the band of intense emission extends over a frequency range from 0.15 to 0.27 f_c as referenced to the local magnetic field. The normalized frequency scale $\tilde{\omega}$ at the bottom of Fig. 8 is the frequency divided by the equatorial value of the cyclotron frequency f_{ce} measured on the same field line using the OTD magnetic-field model (Ness et al. 1986).

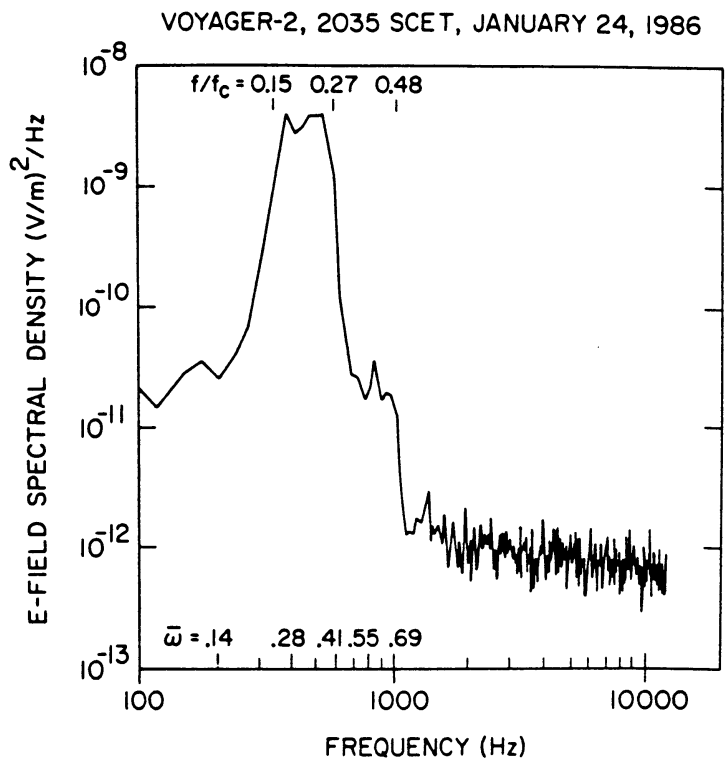

Fig. 8. A 0.6-s average of the wave spectrum from the hiss band shown in Panel *F* of Fig. 7 (Plate 7) showing the detailed form of the hiss band (Coroniti et al. 1987). Notice the extended bandwidth of the emission.

Whistler Theory

Coroniti et al. (1987) have analyzed the effect of the intense whistler-mode hiss on energetic electrons. The result is of fundamental importance to understanding the physics of the Uranian magnetosphere and, specifically, the Uranian aurora. Their line of reasoning is summarized below.

The basis for the theory is the classical work by Kennel and Petschek (1966). The whistlers resonate with energetic electrons. An anisotropy in the resonant part of the electron distribution function provides the free energy source for the waves, and the resulting effect on the electrons is pitch-angle diffusion. The minimum energy for cyclotron resonance with a parallel propagating whistler is

$$R = \frac{B^2}{8\pi n_e}\left(\frac{1-\tilde{\omega}}{\tilde{\omega}}\right)^3 \tag{4}$$

The course taken by Coroniti et al. was to build a model for the plasma based on observations of the electrons. They would then ray trace the generated whistlers from the magnetic equator to the spacecraft, calculating gain along the path. Matching two anisotropy parameters in the model enabled them to obtain the best fit of the gain to the measured spectrum and to calculate a bounce-averaged diffusion coefficient. Given the diffusion coefficient, they went on to calculate scattering lifetimes and compared these to minimum precipitation lifetimes to find the range of energies over which electrons were on strong diffusion. Given the strong diffusion limit, precipitation fluxes and precipitating energy could be calculated and compared with the 10^{11} W required for precipitation of 10-keV electrons needed to drive the observed ultraviolet aurora (Broadfoot et al. 1986).

Coroniti et al. restricted their study to two times, 2011 and 2035 SCET. At 2011 SCET the emissions peaked in the 562-Hz channel of the spectrum analyzer; 2035 SCET was chosen because of the high-resolution wideband data available at the time (see Fig. 8 and panel *F* of Fig. 7 or Plate 3).

The first step in the calculation was to develop a credible model of the plasma in the region between the spacecraft and the magnetic equator. From Eq. 4, it is apparent that the plasma density is an important factor in determining the resonant particle energies. The plasma density profile derived by Kurth et al. (1987) was used as a starting point, but supporting PLS data (McNutt et al. 1987) and independent analysis of the whistler-mode signals themselves were also used. Coroniti et al. used the following formulation for density as a function of *L*:

$$n_e = 2.2(4.8/L)^{1.44}\ \mathrm{cm}^{-3}. \tag{5}$$

The density was assumed to be constant along an *L* shell between the spacecraft and the magnetic equator. This assumption is reasonable since the spacecraft was only about 15° above the magnetic equator during this interval, and no significant populations of heavy ions are present to cause mass loading and related effects.

The whistler-mode emissions imply the existence of large fluxes of energetic electrons with anisotropies that can drive the emissions. Figure 9 shows the fluxes of 22- to 183-keV electrons as observed by the LECP instrument on the same time scale as the spectrum analyzer data and it is clear that intense fluxes of energetic electrons are present at the same time as the intense whistler-mode waves. Unfortunately, the energy range from the 6-keV upper limit of the PLS instrument to the 22-keV lower limit of the LECP instrument is a crucial gap to be included in these considerations and a model for the

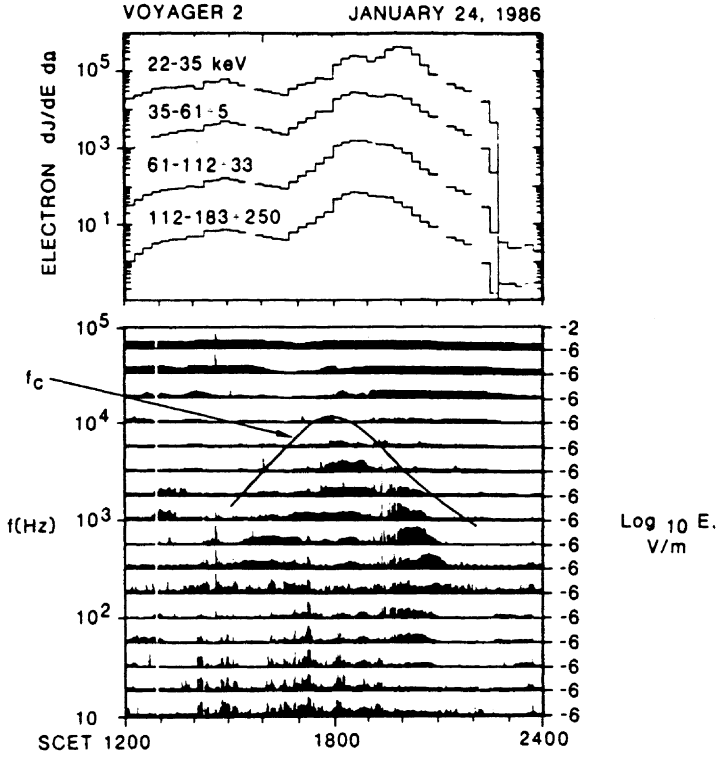

Fig. 9. A comparison of the intensity of the whistler-mode emissions and fluxes of energetic electrons from the LECP investigation (Coroniti et al. 1987). The peak whistler-mode intensities correlate well with the peak fluxes of the energetic electrons.

electrons in this gap was formulated. An anisotropic Maxwellian distribution was assumed for the warm electrons in the gap, matching both the differential flux and the derivative of the differential flux at the 27.5-keV center energy of the lowest energy LECP electron channel. The model is shown by the dashed line in Fig. 10. As a check, the integral flux was compared to that reported by Bridge et al. (1986) and the values matched to within a factor of two.

To explain the relative gain at different frequencies requires that the anisotropy of the warm electrons is different from that of the hot electrons. Since only the anisotropy for the hot electrons is available, a model was assumed which gave a smooth variation in anisotropy over energy with a match at the 27.5-keV center energy of the lowest LECP channel. Hence,

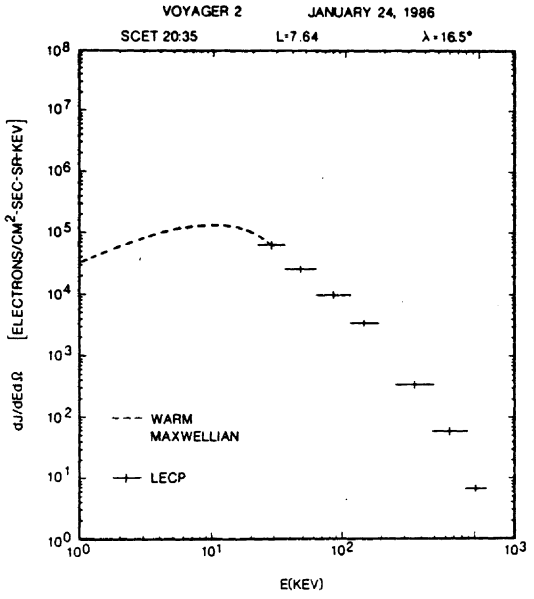

Fig. 10. The model electron distribution used by Coroniti et al. (dashed line) for the whistler-mode interaction calculation (figure after Coroniti et al. 1987).

$$A_w(t) = [A_w(0) - A_E](1 - t^2/t_E^2)^2 + A_E \tag{6}$$

where A_E is the pitch-angle anisotropy (measured), $A_w(t)$ is the anisotropy of the warm electrons as a function of energy, t is energy, and t_E is 27.5 keV. The match condition requires that $A_w(t_E) = A_E$.

The plasma model is then entirely specified by two anisotropies, $A_w(0)$ and A_E. Obviously, the magnetic-field model is also important to the problem: the OTD model of Ness et al. (1986) was used.

The next step in the calculation is to launch the waves from the magnetic equator and calculate the path-integrated gain as a function of frequency. The ray tracing of Coroniti et al. (1987) was accomplished by taking into account the rotation of the whistler-mode wave normal angle due to the curvature in the field and the gradients in the wave index of refraction, following Kimura (1966), Thorne and Kennel (1967), Burtis and Helliwell (1969) and Church (1982). Because of the limited range of latitude required (0 to 16°5) a simple finite differencing scheme was used to do the integration. The gain calculation retained only the first-order cyclotron resonance and the Landau-damping contributions, since these are generally the strongest.

In finding the gain at a given frequency, a variety of initial wave normal

angles was used in order to find the maximum growth. The two anisotropies, $A_w(0)$ and A_E were adjusted iteratively to give the maximum gain as a function of frequency which best matched the observed spectrum. The result of this approach is given in Fig. 11, where the solid dots are the calculated gains and the X's are the measured power spectrum. The two sets of points were normalized by equating the observed and calculated peak-power spectral densities. The anisotropies which provided these fits are A_E = 0.53 (0.56) and $A_w(0)$ = 0.43 (1.1) at 2011 (2035) SCET. A variance analysis was performed which showed that independent variations of 0.1 in the anisotropies seriously degraded the fits.

Differences in the warm-electron model and the effects of launching the waves at locations other than the equator are considered to be minor pertur-

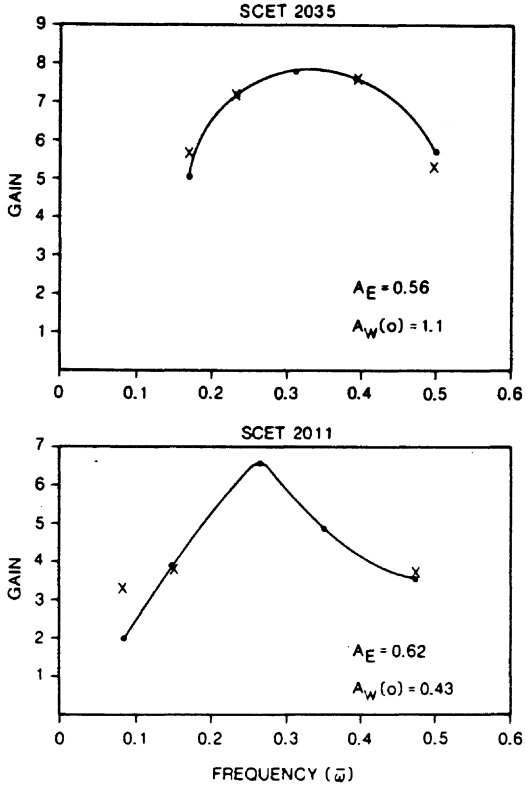

Fig. 11. The results of the fitted gain calculation (dots) compared to the measured gain obtained from the Voyager 2 power spectrum (Coroniti et al. 1987).

bations to the calculation; the actual calculation simply shows the consistency between the observations and the amplification model.

The nonrelativistic diffusion coefficient for parallel whistlers can be written as

$$D_{\alpha\alpha} = 4.4 \times 10^4 n^2 E^2(f) \left| \frac{v_g}{v_g + |v_\parallel|} \right|_{\omega = \omega_r} \tag{7}$$

where n is the index of refraction and v_g is the group velocity. Since a whistler will resonate with different energy electrons as it traverses the region of growth, one must calculate a bounce-averaged diffusion coefficient.

The average pitch-angle scattering time T_s is roughly the inverse of $D_{\alpha\alpha}$ and the electron fluxes will be at or close to the strong diffusion limit if $T_s < T_{min} = 4L^4 R_U / v_\parallel$, the minimum precipitation lifetime (Kennel 1969). Coroniti et al. presented the results of the T_s vs T_{min} comparison as in Fig. 12. It is readily apparent that the bounce-averaged scattering times are below the minimum precipitation lifetimes for a wide range of electron energies at both times. Electrons in the energy range of about 5 to 40 keV are apparently on strong diffusion for this time interval on L shells of about 6 to 9.

Following Coroniti and Kennel (1970) the precipitating electron flux J_p is related to the trapped flux J_T approximately by

$$\frac{J_p}{J_T} = \frac{T_{min}}{T_L} \tag{8}$$

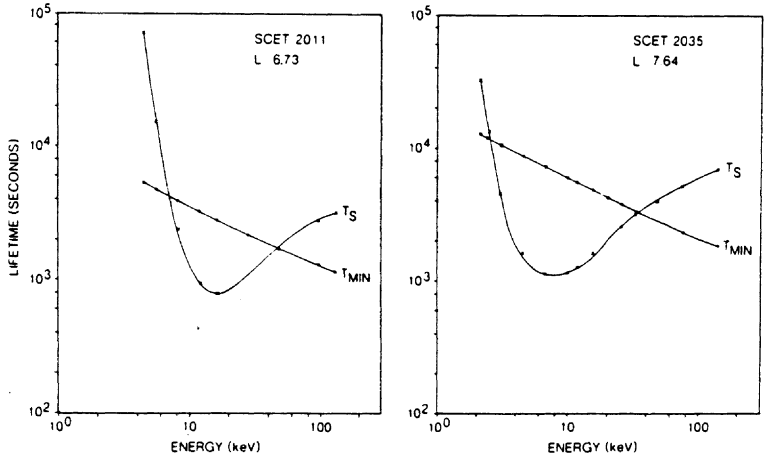

Fig. 12. A comparison of the scattering time T_s calculated from the bounce-averaged diffusion coefficient and T_{min}, the minimum precipitation lifetime (Coroniti et al. 1987). When the scattering time is less than T_{min}, the electrons are precipitating at or near the strong diffusion limit.

where T_L is the electron lifetime which is approximately equal to T_{min}. Hence, the total precipitating energy flux at 2011 SCET ($L = 6.73$) is about 1.0 erg cm^{-2} and at 2035 SCET ($L = 7.64$) the precipitating energy flux is about 0.5 erg cm^{-2}. Since the precipitating flux appears to increase with decreasing L and the intense waves exist over the range of about $L = 6$ to 9, it is possible that the energy flux into the atmosphere exceeds 1.0 erg cm^{-2} at $L = 6$. Broadfoot et al. (1986) reported auroral luminosity near the southern magnetic pole that would require approximately 10^{11} W from precipitating electrons in the 10-keV energy range. Coroniti et al. (1987), assuming a uniformly illuminated 20° polar cap, estimated this to be about 0.8 erg cm^{-2}, very close to the calculated precipitating energy fluxes.

As pointed out by Cheng et al. in their chapter, as well as in Coroniti et al. (1987), the above result leads to some interesting problems. The strong diffusion implies there is a very strong source of a few to 50-keV electrons. Cheng et al. (1987*b*) find the radial diffusion coefficient to be 10^{-6} to 10^{-7} s^{-1} at $L = 7.5$. For strong diffusion, we require $D_{LL}T_{min} > 1$ which leads to $D_{LL} \simeq 2.5 \times 10^{-4}$ s^{-1}. One possible explanation for this discrepancy would be that there exist strong temporal variations in the fluxes, or substorm-like injections of 5- to 40-keV electrons. Mauk et al. (1987), Cheng et al. (1987*b*) and Sittler et al. (1987) all presented evidence for injections, but Cheng et al. argued against substantial injection events based on the near equality of the inbound and outbound electron phase-space densities at $L = 10$.

The precipitation lifetime calculations of Coroniti et al. (1987) are based on the assumptions that:

1. All the electric-field intensity measured is due to whistler-mode waves;
2. The electric fields are primarily transverse to the Uranian magnetic field;
3. The index of refraction (based primarily on the electron density) is well known;
4. The turbulence exists throughout the ± 16° region;
5. The diffusion rate must be maintained along the drift/transport trajectory for at least T_{min}.

The first two assumptions are based almost purely on terrestrial experience. The electron density is consistent with three independent estimates, including those of McNutt et al. (1987), Kurth et al. (1987) and Coroniti et al. (1987). The good agreement between the ray-tracing calculations of the path-integrated gains and the observed waves leave little doubt that the amplification region must fill the 16° region between the spacecraft and the magnetic equator. Finally, the continuously present band of intense whistler-mode emissions over the interval from 1950 SCET to 2100 SCET argues strongly that the turbulence is widespread and continuous enough to meet the T_{min} criterion. We conclude that the precipitation lifetimes are reasonable.

One other conflicting factor one should consider is that the location cited for the strong Uranian radio emissions (cf. Leblanc et al. 1987; Kaiser et al.

1987; Zarka and Lecacheux 1987) is generally on much larger L shells, close to 15 to 20. Given that the radio emissions are driven by an auroral process, it is difficult to reconcile the auroral precipitation on much lower L shells. On the other hand, Barbosa (1988) suggests that the intense radio emission is likely on much lower L values near $L = 4$, and Romig et al. (1987) suggested a source near $L = 5$, more consistent with those associated with the strong whistler-mode diffusion discussed here.

Coroniti et al. (1987) offered one other possible explanation for the large energetic electron fluxes implied by the whistler-mode emissions. They suggested that low-energy electrons could experience strong upward energy diffusion prior to being lost to the atmosphere. Significant work would be required to explore fully the mechanism, which is based on the work of Kennel (1969).

Most recently, Mauk et al. (1989) reported an unusual electron signature at the minimum L shell of Ariel which could be interpreted as being due to the loss of 22- to 35-keV electrons by impact with micron-sized dust grains in Ariel's orbit. Their interpretation leads to the conclusion that the electrons could not be on strong diffusion and still show the observed signature. This interpretation offers a fresh view on the question of strong diffusion. However, questions remain about Mauk et al.'s interpretation of the signature, which is not a unique result and which poses a number of other difficulties. The question of whether electrons are truly on strong diffusion in the Uranian magnetosphere will not be resolved without significant further analysis and possibly not without additional observations.

V. PLASMA WAVES IN THE MAGNETOTAIL

The magnetotail of Uranus is characterized by low levels of plasma wave turbulence (Gurnett et al. 1986), contrary to the situation at Earth. Observations of waves in the Uranian magnetotail were reported by Kurth et al. (1989); those waves are reviewed in this section. Unfortunately, the Voyager observations are not sufficient to settle satisfactorily upon the wave mode most dominant in the magnetotail.

Observations

Figure 13 presents an overview of the observations of plasma waves in the magnetotail of Uranus. The figure spans the time from closest approach to the approximate occurrence of the fourth and partial encounter with the plasma sheet (Ness et al. 1986). Much more data exist between the end of Figure 13 and the magnetopause crossing, but little or no plasma wave activity is identifiable in the outer portion of the magnetotail trajectory. The D at the top of Fig. 13 locates the abrupt decrease in the fluxes of energetic particles in the Uranian radiation belts (Mauk et al. 1987). Hence, the wave events of interest for magnetotail studies are found later in time than D. One

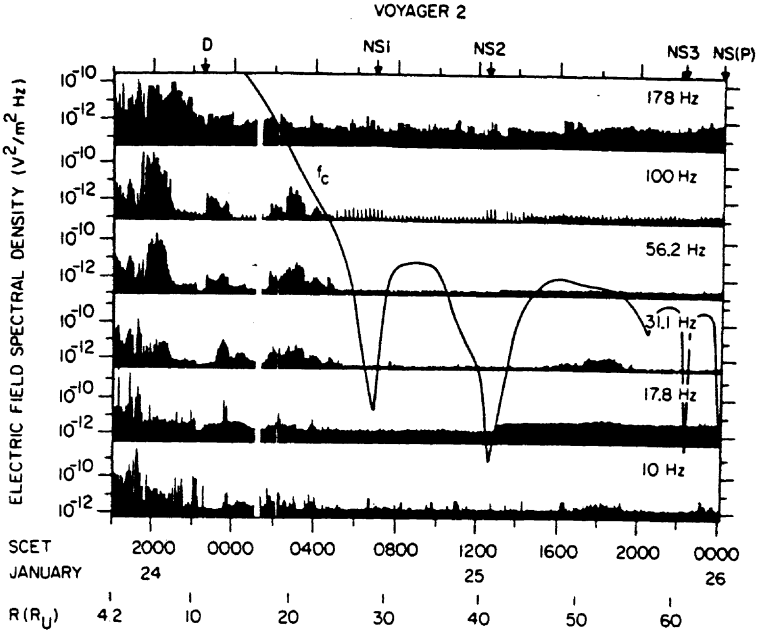

Fig. 13. An overview of the low-frequency waves observed in the magnetotail of Uranus. Notice that the activity is confined to frequencies below f_c and are observed before the first and after the second neutral sheet crossing (figure from Kurth et al. 1988).

can identify three regions of magnetotail wave activity. These are centered near 2300 SCET on January 24 and 0300 and 1800 SCET on January 25, 1986. These events are confined to extremely low frequencies and in each case appear to be limited on the high-frequency side by the contour of f_c.

An additional observation can be made about the three wave events in Figure 13. The turbulence occurs before the first neutral sheet crossing (NS1) (Ness et al. 1986), and after the second crossing (NS2). The wave activity is well separated from the magnetic-field strength minima associated with the neutral sheet. Comparisons with PLS and LECP observations also indicate the second and third wave events are not associated with the plasma sheet. It is interesting that the activity does not appear between NS1 and NS2, when the spacecraft would be on field lines connected to the dayside, northern magnetic pole.

Figure 14 shows spectra typical of those observed in all three of the magnetotail wave events. Those shown are from the second event, near 0200 SCET on January 25. Plotted are 5-min average spectra and the peak values observed over the same 5-min interval for two time periods. Both sets of spectra show evidence for a local maximum in the spectrum at about 56 Hz,

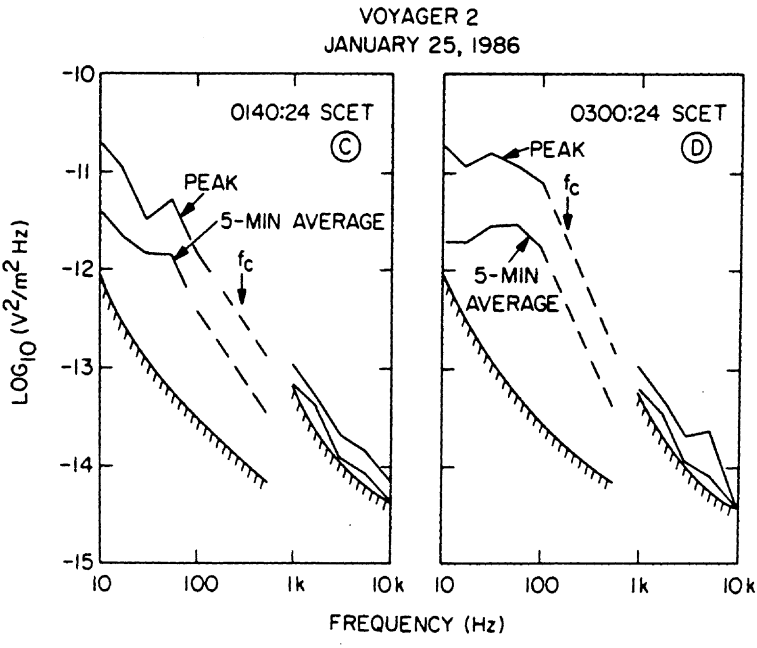

Fig. 14. Typical spectra of the waves observed in the magnetotail. The spectra are reminiscent of broadband electrostatic waves in the terrestrial magnetosphere (figure from Kurth et al. 1989).

but the spectrum from 0140 SCET (labeled *C*) is almost monotonically decreasing in frequency. Spectra taken from the third event near 1800 SCET on January 25 do show a simple monotonically decreasing trend and no evidence for a local maximum.

Interpretation of the Magnetotail Waves

The absence of a Voyager magnetic sensor sensitive to frequencies up to 100 Hz complicates the analysis of the waves observed in the Uranian magnetotail. The fact that the spectrum lies below f_c and the likelihood that $f_p > f_c$ means that the wave spectrum is at least consistent with whistler-mode emissions. The other competing interpretation for the waves, given by Kurth et al. (1989), is that they are analogous to the broadband electrostatic noise common in the terrestrial magnetosphere. The spectra shown in Fig. 14 are reminiscent of those taken at Earth by Gurnett et al. (1976) and Gurnett and Frank (1977).

Further indication that the waves are more like broadband electrostatic noise than whistler emissions comes from an analysis of the locations of the event. Figure 15 shows the location of wave activity against a cartoon model of the plasma sheet taken from Mauk et al. (1987). The last three darkened

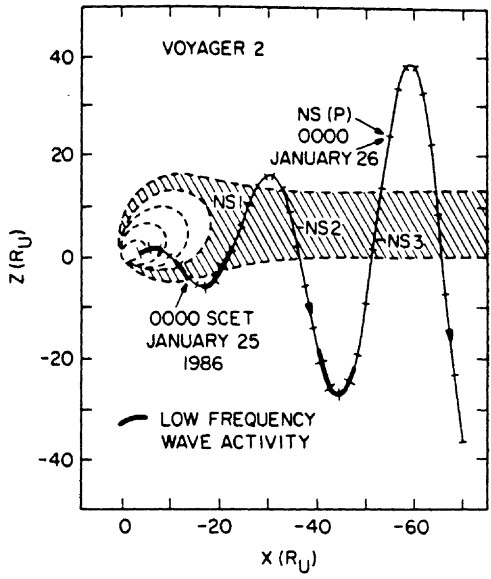

Fig. 15. A schematic drawing of the Uranian plasma sheet taken from Mauk et al. (1987) showing the locations of the plasma-wave activity (from Kurth et al. 1989). Notice the waves are confined to the southern magnetic hemisphere.

portions of the Voyager 2 trajectory in this solar-magnetospheric coordinate system correspond to the three wave events from Fig. 13. The first of these corresponds very well to the "horn" of the plasma sheet and the second could be construed as having a relation to the plasma sheet boundary layer. According to this construction, the third event lies deep in the magnetotail lobe, although it is possible for this event to be in the magnetopause boundary layer. Scarf et al. (1984) reported broadband electrostatic noise in a similar region at the Earth. The three events thus occur in regions of the magnetosphere similar to the known locations for broadband electrostatic noise seen in terrestrial observations. Figure 15 shows that the wave activity favors the nightside, southern magnetic field lines, suggesting an asymmetry with the dayside, northern magnetic field lines. Such asymmetries are common in other phenomena observed at Uranus. The main Uranian radio emissions almost certainly are associated with the southern magnetic pole (cf. Leblanc et al. 1987; Kaiser et al. 1987; Zarka and Lecacheux 1987).

The broadband electrostatic-wave interpretation for the magnetotail waves suggests that field-aligned ion beams or current instabilities might be responsible for driving the waves (Grabbe and Eastman 1984; Omidi 1985; Dusenbery and Lyons 1985; Ashour-Abdalla and Okuda 1986; Akimoto and Omidi 1986). Kurth et al. (1988) looked for evidence of field-aligned ion

flows in the LECP data and did find evidence for such distributions. However, the detailed comparison of the LECP flow observations with the occurrence of the wave events was not sufficient to allow a solid correlation to be made.

In summary, it is unfortunate that Voyager 2 did not provide additional information on the nature of the waves observed in the Uranian magnetotail, since a definitive identification of the mode is difficult or impossible without such information. It is important to observe the presence of the emissions and to note that their locations are remote from the neutral sheet. The implication is that interesting physical processes occur in all parts of the Uranian magnetosphere, as is the case at Earth.

VI. SUMMARY

This chapter presents a discussion of the primary plasma waves observed in the Uranian magnetosphere. It is important to consider that the scope of the chapter is influenced strongly by the preceding work on the Uranian plasma-wave observations. There are other emissions that have not been discussed here, such as the unexplained bursty emissions near the outbound Miranda L-shell crossing (Kurth et al. 1986), lower hybrid waves in the vicinity of the more intense whistler-mode emissions (Coroniti et al. 1987), and others which are still poorly understood.

The waves discussed include upstream Langmuir waves and turbulence at the bow shock, Bernstein electrostatic waves, whistler-mode chorus and hiss, and low-frequency turbulence in the magnetotail, tentatively identified as broadband electrostatic noise. Figure 16 is a schematic representation of the magnetosphere in which the locations of these major plasma-wave types are identified. It is important to remember while studying Fig. 16 that Voyager 2 sampled only a very small volume of the space represented. Considerable liberty has been taken in identifying the various regions.

The upstream Langmuir waves represent the most distant form of wave-particle interactions associated with the magnetosphere of Uranus and are remarkable because of their extensive sphere of influence. In addition to those located in the general solar direction, similar emissions were also observed beyond the dawn flank of the magnetosphere during the outbound portion of the trajectory. The turbulence at the bow shock has many similarities to shock spectra at Jupiter and Saturn if one takes into account the downward shift of critical frequencies of the solar-wind plasma associated with the greater heliocentric distance of Uranus. One remarkable characteristic of the outbound bow-shock spectra is the notch between the whistler-mode turbulence and the ion-acoustic turbulence. While studies of the shocks at Jupiter and Saturn (Moses et al. 1985,1988) might lead one to expect that the shock turbulence plays an important role in heating electrons, recent analyses (Moses et al. 1989) indicate that the Uranian wave intensities are too low for significant heating.

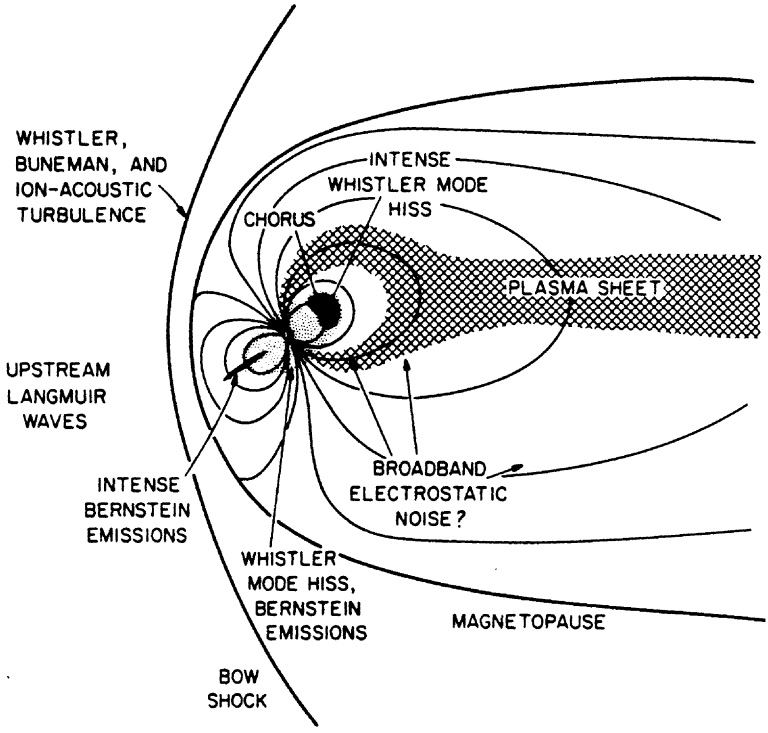

Fig. 16. A schematic summary of the locations of various plasma-wave phenomena detected in and near the magnetosphere of Uranus. Note that the limited spatial coverage of the Voyager 2 trajectory affects the accuracy of such a graph. (Figure adapted from Behannon et al. 1987 and Mauk et al. 1987).

The Bernstein waves are pervasive in the inner portion of the magnetosphere. As in the other planetary magnetospheres, these waves have their maximum intensities at the magnetic equatorial plane. The wave amplitudes were modest by terrestrial standards, but because Voyager 2 did not cross the magnetic equator inside of about 11.5 R_U, it is possible that significantly more intense Bernstein emissions exist. At Earth, these emissions are at least partially responsible for scattering electrons from the plasma sheet into the loss cone to produce the diffuse aurora. Given that significant intensities ($\sim$ 1 mV m^{-1}) occur for these bands near the equator in the Uranian inner magnetosphere, they could play a role as a loss mechanism for radiation-belt electrons with energies of a few keV.

The most significant wave activity at Uranus is the whistler-mode band which permeates the inner magnetosphere, where the electron fluxes are high. In the outbound region on L shells of 6 to 9, the waves are sufficiently intense

to put 5- to 40-keV electrons on strong diffusion and could, therefore, produce the observed ultraviolet aurora. Unfortunately, it is not clear how the energetic electrons are resupplied fast enough to support this process in view of the scattering lifetimes of order 10^3 s. A complete understanding of the ongoing processes in the Uranian magnetosphere cannot be had until the role of these waves is fully reconciled with other independent estimates of the diffusion coefficient. Several possibilities exist for this reconciliation, including time-variable injections or upward-energy diffusion of the electrons prior to precipitation. These require further consideration.

The final class of waves considered here are the weak low-frequency emissions noted in the horn of the plasma sheet and in the magnetotail. While the whistler mode cannot be ruled out for these waves, Kurth et al. (1989) favor a broadband electrostatic noise interpretation for the emissions. Such an interpretation fits the terrestrial situation of electrostatic noise observed in conjunction with field-aligned ion flows near the plasma sheet, near magnetopause boundary layers, and on auroral field lines closer to the planet.

In view of the unlikely possibility of returning to Uranus in the near future, it is folly to discuss goals for additional plasma wave observations there. Nevertheless, several issues raised herein demand attention. The primary one is to provide answers for the questions raised by the strong diffusion by whistler-mode waves. Certainly an orbiter with a periapsis of 4 R_U or less would be able to sort out the apparent asymmetries in whistler-mode intensities and be able to attribute rigorously variations to either temporal or spatial effects. Accompanying energetic electron observations could better characterize substorms or injection effects. Associated observations would have to include high-resolution maps of the auroral region and its temporal variations as well as a definitive study of the location of the various radio sources, particularly those associated with the aurora.

Another high-priority reason for a return to Uranus would be to cover the magnetic equatorial region close to the planet in order to assess better the importance of the Bernstein emissions and their potential as a loss mechanism for energetic particles. Even for those emissions measured near 11.5 R_U there is little confidence in the resonant energy of electrons that interact with those waves because of the low electron fluxes measured during that event (Sittler et al. 1987). These emissions are also good candidates for the source of the weak continuum radiation observed by Gurnett et al. (1986) and Kurth et al. (1990) and could also be related to the sporadic narrowband radio emissions near 5 kHz (Kurth et al. 1986).

While many other issues could benefit from a return flight to Uranus, a final one, which is especially enticing, is to understand the dramatic change in the plasma wave spectrum observed by Voyager 2 near 1930 SCET on January 24. Was this change related to the spacecraft passage through the Miranda L shell, or alternatively, to spacecraft passage through the convection limit (McNutt et al. 1987; Selesnick and McNutt 1987)? It was within this

region that Voyager observed an almost complete drop-out of the otherwise omnipresent whistler band and saw it replaced with very bursty, still unexplained emissions. Kurth et al. (1986) also associated this region with the source of the sporadic narrowband radio emissions and the bursty nature of the plasma waves in this region may also relate to the higher-frequency bursty radio emissions (Warwick et al. 1986; Evans et al. 1987).

Finally, it should be recognized that a return mission to Uranus will find a dramatically different magnetosphere due to the large variations in Sun-magnetic dipole directions over the Uranian year. It would be extremely illuminating (and not solely from the point of view of wave-particle interactions) to observe changes in the magnetosphere over a significant fraction of the Uranian orbit around the Sun.

Acknowledgments It is unfortunate that Fred Scarf did not live to see the completion of this work. Nevertheless, he made this chapter possible and contributed greatly to its content. His absence will be sorely felt, but we will strive to continue his pioneering spirit in the Voyager adventures to come. The research at the University of Iowa was supported by the National Aeronautics and Space Administration through a contract with the Jet Propulsion Laboratory. Likewise the research at TRW was supported by NASA through a contract with JPL.